PERGAMON

International Journal of Solids and Structures 36 (1999) 1045–1079

INTERNATIONAL JOURNAL OF SOLIDS and STRUCTURES

An Element Free Galerkin analysis of steady dynamic growth of a mode I crack in elastic–plastic materials

Yu Xu*, Sunil Saigal

Department of Civil and Environmental Engineering, Carnegie Mellon University, PA 15213, U.S.A.

Received 1 November 1996; in revised form 20 October, 1997

Abstract

An Element Free Galerkin (EFG) method based formulation for steady dynamic crack growth in elastic–plastic materials is developed. A domain convecting parallel to the steadily moving crack tip is employed. The EFG methodology eliminates the stringent mesh requirements of the Finite Element Method (FEM) for such problems. Both rate-independent materials and rate-dependent materials are considered. The material is characterized by von Mises yielding condition and an associated flow rule. For rate-independent materials, both the influence of crack speeds and that of strain hardening on the mechanics of steady dynamic crack growth are investigated. For rate-dependent materials, only a non-hardening material is considered with emphasis on determining the influence of viscous properties of materials and crack speeds. The influence of strain hardening on steady dynamic crack growth shows the same trends as for steady quasi-static crack growth. The simplifications used in the literature in deriving analytical solutions for high strain-rate crack growth have been examined thoroughly using the numerical results.

1. Introduction

Steady dynamic growth of a mode I crack under plane strain conditions has been investigated for different types of nonlinear material behaviors in the literature, e.g. the elastic–plastic materials and the elastic–viscoplastic materials. For the former, simple material models, such as an elastic–perfectly plastic material, or an elastic–plastic material with bilinear stress–strain relation or an elastic–perfectly incompressible material have been employed in Achenbach et al. (1981a), Achenbach and Dunayevsky (1981b), Gao and Nemat-Nasser (1983) and Leighton et al. (1987). The emphasis in these studies has been on determining the effect of crack speeds. For elastic–viscoplastic materials, simple material models, such as a linearly-viscous plastic model, have been

* Corresponding author.

0020–7683/99/$ - see front matter
PII: S0020–7683(97)00337–5

considered and the emphasis has been on the study of the viscous effects of these materials (see e.g. Freund and Hutchinson, 1985; Mataga et al., 1987). Compared to the investigations on steady quasi-static growth of mode I cracks in an elastic–plastic material, not many numerical investigations of steady dynamic growth of mode I cracks are available in the literature. The available analytical investigations have either relied on simplifying approximations (see e.g. Achenbach et al., 1981a; Achenbach and Dunayevsky 1981b; Freund and Hutchinson, 1985; Mataga et al., 1987) or focused on the incompressible materials (see e.g. Gao and Nemat-Nasser, 1983; Leighton et al., 1987).

A few asymptotic analyses of steady dynamic growth of a mode I crack in an elastic–perfectly plastic material have been made. Considering elastic compressibility of materials, both Slepyan (1976) and Achenbach and Dunayevsky (1981b) derived asymptotic near-tip stress and deformation fields. Their solutions are only applicable when the crack speed is small compared to the shear wave speed of the material. In their analysis, while the Tresca yielding condition was used, the Mises flow rule was employed to relate the plastic strain component increments and the deviatoric stress components. Focusing on incompressible materials, Gao and Nemat-Nasser (1983) found discontinuities of stress and velocity along lines radial from the crack tip which occur at all crack speeds. In their analysis, the Mises yielding condition and the associated flow rule was used. Furthermore, Leighton et al. (1987) demonstrated the inconsistency between the discontinuities of stress and velocity fields and the principle of maximum plastic work. For steady dynamic crack growth in an elastic–perfectly plastic incompressible material obeying the Tresca yielding condition and the associated flow rule, Leighton et al. (1987) constructed an asymptotic solution valid for all crack speeds. In their asymptotic solution, the stress, strain and particle velocity components are continuous. However, their asymptotic solution does not reduce to the asymptotic solution for the quasi-static case given by Drugan et al. (1982) as the crack speed approaches zero. According to Leighton et al. (1987), the domain of validity of their asymptotic solution vanishes as the crack speed approaches zero. Also, there is no elastic unloading zone in the solution of Leighton et al. (1987).

There are not many numerical studies in the literature on steady dynamic growth of mode I cracks in an elastic–plastic material under plane strain conditions. Using an approach similar to those proposed by Dean and Hutchinson (1980) and Parks et al. (1981), Lam and Freund (1983, 1985) studied the influence of crack speeds on the stress and deformation fields near a steadily moving crack. In Lam and Freund (1983, 1985), no results including strain hardening effects were reported. The material was assumed to be elastic–perfectly plastic and was characterized by the Mises yielding condition and the associated flow rule. They found that inertia (or crack speed) has a significant effect on the elastic–plastic response of material particles near the crack tip, and the elastic unloading may occur behind the crack for higher speeds.

Both analytical and numerical investigations of steady dynamic growth of a mode I crack in viscoplastic materials have received considerable attention in the past decade. This problem is of significant interest since the material particles near the rapidly running crack tip experience a remarkably high strain-rate deformation, and the material resistance to plastic flow increases dramatically at high strain-rates.

For steady dynamic growth of a mode I crack in rate-dependent materials characterized by an elastic/power law viscoplastic model, Lo (1983) and Brickstad (1983) found that the asymptotic near-tip stress field in the high strain-rate zone is uniquely dominated by the local crack-tip stress

intensity factor K_{tip}, in the same singularity form as the asymptotic dynamic elastic stress field given by Freund (1976) as long as the stress exponent is less than three, except that an amplitude below the elastic dynamic intensity factor K results due to plastic dissipation. Thus, the near-tip stress field can be expressed as (see Freund and Hutchinson, 1985)

$$\sigma_{ij} = \frac{K_{\text{tip}}}{\sqrt{2\pi r}} \Sigma_{ij}(\theta, m) \quad r \to 0 \tag{1}$$

where r, θ are planar polar coordinates centered at the tip; $m = v/c_r$ is the crack Mach number; v and c_r are the speeds of the crack tip and the Rayleigh wave, respectively; Σ_{ij} are universal functions for a given mode which may be found in Freund and Hutchinson (1985); K_{tip} is related to the crack-tip energy release-rate G_{tip} for a mode I loading as (see Freund and Hutchinson, 1985)

$$G_{\text{tip}} = f(m) \frac{(1-v^2)}{E} K_{\text{tip}}^2 \tag{2}$$

where $f(m)$ may be found in Freund and Hutchinson (1985). The near-tip behavior of the high strain-rate crack in rate-dependent materials is characterized by the above formula. The objective in both analytical and numerical studies is to relate the crack-tip energy release-rate G_{tip} and the overall energy release-rate G which represents the overall crack driving force. The influence of the parameters of the viscoplastic material model and that of crack speed on this relationship are also of interest. Freund and Hutchinson (1985), starting with a constitutive equation that governs plastic flow in two regimes: a low strain-rate regime where the yield stress in shear is a constant, and a high strain-rate regime where the yield stress in shear is a linear function of the shear plastic strain-rate, presented a simple closed form expression for G_{tip} in terms of the parameters of the viscoplastic material model, the crack speed, and the overall energy release-rate G. Based on their numerical analysis, Mataga et al. (1987) proposed a modified formula for the crack-tip energy release-rate G_{tip}.

Steady dynamic crack growth in rate-dependent materials has also been studied numerically. Using a finite element formulation similar to Dean and Hutchinson (1980) and Parks et al. (1981), Freund et al. (1986), Mataga (1986) and Mataga et al. (1987) numerically investigated the problem of Freund and Hutchinson (1985). In these numerical studies, the relationship between G_{tip} and G was examined. As reported in Mataga et al. (1987), they also observed that the original relation given by Freund and Hutchinson (1985) underestimates plastic dissipation while the modified relation given by Mataga et al. (1987) overestimates it. Similar analysis was also performed by Ostlund (1990), but with an emphasis on the size of the near-tip elements required to obtain reliable results. Shenoy and Krishna (1994) obtained a quantitative relationship between the dynamic fracture toughness and the crack speed for this problem.

The finite element method has been extensively employed for the numerical studies of crack problems. The conventional FEM does not provide a high resolution of localized steep gradients near the tip for such problems. Singular elements introduced to model steep gradients in Akin (1976) do not improve the numerical performance for steady crack growth problems (see Ostlund, 1990). Very fine elements have to be used around the crack tip to capture the asymptotic feature of the respective stress and deformation fields. The steady state condition, preferably, requires the use of rectangular elements, all of the same height, in the plastic zone leading to elements of an

undesirable shape. Furthermore, an ill-conditioned stiffness matrix may result due to a large variation in the size of elements used. Therefore, using conventional finite element analysis for steady crack growth may lead to a conflicting situation: refining the mesh near the crack tip may lead to improved accuracy; while this may result in an ill-conditioned stiffness matrix leading to a loss of accuracy of the solution. The difficulties associated with the FEM in numerical investigations of steady crack growth justify the need to look for other high-accuracy numerical methods that also avoid the above conflicting situation in the finite element analyses.

The Element Free Galerkin (EFG) method has recently been applied for the analysis of crack growth problems (see e.g. Xu, 1996 and the references listed there). Compared to the FEM, the EFG method can achieve high resolution of localized steep gradients and be very effective for crack growth problems (see e.g. Xu, 1996; Xu and Saigal, 1997a, b, and the references listed there). Coupled with an extension of the convective mesh technique, the EFG method has been employed to simulate steady dynamic crack growth of mode I cracks in an elastic material under plane strain conditions (see Xu, 1996; Xu and Saigal 1997a). The numerical predictions for the stress intensity factor K, the energy release rate G, the near-tip fields, and the crack opening profiles agree well with the analytical results. The results from EFG analyses were earlier found to be more accurate than the corresponding FEM solutions in Xu (1996) and Xu and Saigal (1997a). The EFG method has also been applied to simulate steady quasi-static growth of mode I cracks in an elastic–plastic material under plane strain conditions in Xu (1996) and Xu and Saigal (1997b). For this study the numerical solution predicts the existence of an elastic unloading wedge which was also predicted by Drugan et al. (1982). A good agreement with the asymptotic near-tip stress field of Drugan et al. (1982) was also observed and an estimate for the range of validity of the asymptotic solution of Drugan et al. (1982) was developed.

The steady dynamic growth of mode I cracks in an elastic–plastic material or an elastic–viscoplastic material is studied in this paper. A numerical scheme based on the extension of the convective mesh technique and the EFG method is employed in this study. Under the assumption of small scale yielding, a remote elastic stress or deformation field was imposed on the boundaries of the domain under consideration, which is of a size much larger compared to the size of the active plastic zone. The material is characterized by von Mises yielding condition and an associated flow rule. Both rate-independent materials and rate-dependent materials are considered. For rate-independent materials, both non-hardening materials and hardening materials are considered. For strain-hardening, both linear hardening and power-law hardening models are employed. To the best knowledge of the authors, no numerical results concerning steady dynamic crack growth in hardening materials have been reported in the literature to date. In the present study, numerical results show a good agreement with the asymptotic near-tip stress field for cracks growing with a small speed in an elastic–perfectly plastic material. The elastic unloading zone was predicted by the numerical solutions. For rate-dependent materials, the material was assumed to be rate-independent elastic–perfectly plastic when the plastic shear strain-rate is under a threshold value. Above the threshold, the material was considered to be viscoplastic with the yield stress in shear depending linearly on the plastic shear strain-rate (see Freund and Hutchinson, 1985; Mataga et al., 1987). A detailed examination of the assumptions employed in deriving the analytical expression available in Freund and Hutchinson (1985) was made. An extensive comparison of the relation of the crack-tip energy release-rate G_{tip} to the overall energy release-rate G obtained from numerical predictions and analytical results, respectively, was made.

2. Numerical formulation

The typical descriptions of steady dynamic crack growth in rate-independent materials and rate-dependent materials are shown in Figs 1(a) and (b), respectively. A Cartesian system for which the crack edge coincides with the $\bar{x}_3$ axis, and propagates along the $\bar{x}_1$ axis with a constant speed $\bar{v}$ is employed. The coordinates system $\{\bar{x}_1, \bar{x}_2, \bar{x}_3\}$ is considered to be moving with its origin always at the crack tip. A state of plane strain deformations is assumed. All variables are then independent of $\bar{x}_3$, and the displacement in the $\bar{x}_3$ direction is zero. Using the steady state condition, the material time derivative of the Cartesian component of any vector or tensor may be replaced by the $\bar{x}_1$-gradient as

$$\frac{\partial}{\partial t} = -\bar{v}\frac{\partial}{\partial \bar{x}_1} \tag{3}$$

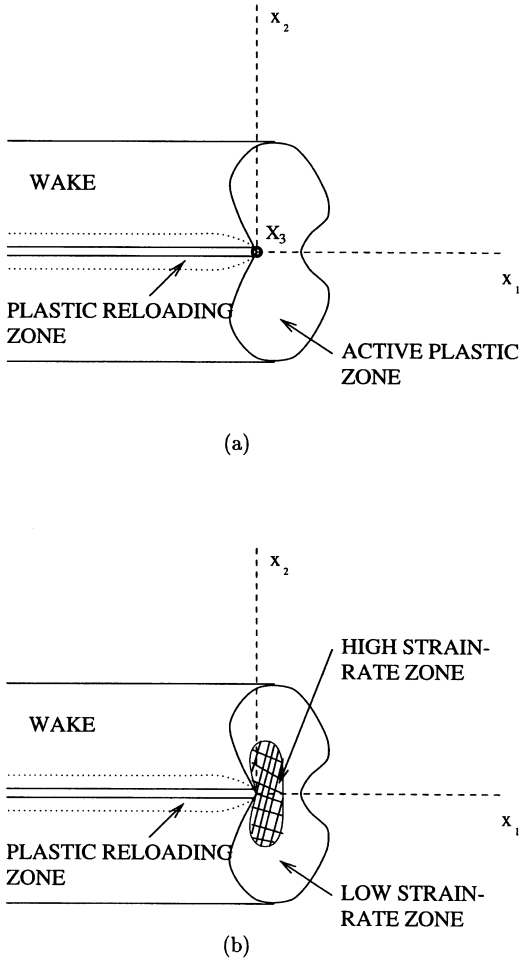

Fig. 1. Steady dynamic crack growth: (a) in rate-independent materials and (b) in rate-dependent materials.

where $\bar{v}$ is the speed of the crack tip. Employing the non-dimensional quantities $x_i = \bar{x}_i/l$, $u_i = \bar{u}_i/(\tau_y l/\mu)$, $\sigma_{ij} = \bar{\sigma}_{ij}/\tau_y$, $\varepsilon_{ij} = \bar{\varepsilon}_{ij}/(\tau_y/\mu)$ where μ is the elastic shear modulus, τ_y is the yield stress in shear, $l = \mu G/\tau_y^2$ is the characteristic length and G is the overall energy release rate of the crack, the momentum equation, using eqn (3), can be written in the non-dimensional form as

$$\sigma_{ij,j} = m_s^2 u_{i,11} \tag{4}$$

where $m_s = \bar{v}/c_2$ is the non-dimensional crack speed, and $c_2 = \sqrt{\mu/\rho}$ is the elastic shear wave speed of the material.

The weak form corresponding to the momentum relation in eqn (4) is given as

$$\int_\Omega \delta v_{i,j}\sigma_{ij}\,\mathrm{d}\Omega - \int_\Omega m_s^2 u_{i,1}\delta v_{i,1}\,\mathrm{d}\Omega + \int_\Gamma m_s^2 n_1 u_{i,1}\delta v_i\,\mathrm{d}\Gamma + \int_{\Gamma_t}\delta v_i t_i^*\,\mathrm{d}\Gamma - \int_{\Gamma_u}\delta v_i\lambda_i\,\mathrm{d}\Gamma - \int_{\Gamma_u}\delta\lambda_i(u_i - u_i^*)\,\mathrm{d}\Gamma = 0 \tag{5}$$

where Ω is the convective domain under consideration; Γ is the boundary of the domain Ω; n_1 is the component of the unit normal to the boundary Γ in the x_1 direction; and t_i^* and u_i^* are the prescribed tractions on traction boundaries Γ_t and the prescribed displacements on displacement boundaries Γ_u, respectively. Since moving least squares interpolants (see e.g. Belytschko et al., 1994; Xu, 1996 and the references listed therein) are employed, it is not possible to prescribe the displacement boundary conditions directly. Instead, Lagrange multipliers, λ_i, are used to impose the displacement boundary condition in the weak form given above. As long as the above weak form is valid for arbitrary test functions δv_i and $\delta\lambda_i$ subject to the usual admissibility conditions, the momentum equation and the boundary conditions are satisfied.

Under the context of small strain theory, the non-dimensional strain ε_{ij} can be expressed as the sum of elastic strain ε_{ij}^e and plastic strain ε_{ij}^p as

$$\varepsilon_{ij} = \varepsilon_{ij}^e + \varepsilon_{ij}^p \tag{6}$$

The nondimensional stress at the same point is given as

$$\sigma_{ij} = C_{ijkl}(\varepsilon_{kl} - \varepsilon_{kl}^p) \tag{7}$$

or in the matrix form as

$$\{\sigma\} = \{\mathbf{D}^e\}(\{\varepsilon\} - \{\varepsilon^*\}) \tag{8}$$

where C_{ijkl} is the non-dimensional elasticity tensor, $\{\mathbf{D}^e\}$ is the non-dimensional elastic constitutive matrix (see e.g. Xu, 1996), and

$$\{\sigma\} = \begin{Bmatrix}\sigma_{11}\\ \sigma_{22}\\ \sigma_{12}\end{Bmatrix}, \quad \{\varepsilon^*\} = \begin{Bmatrix}\varepsilon_{11}^p - \nu\varepsilon_{33}^p\\ \varepsilon_{22}^p - \nu\varepsilon_{33}^p\\ \varepsilon_{12}\end{Bmatrix} \tag{9}$$

Note that $\{\varepsilon^*\}$ is different from $\{\varepsilon^p\}$ as long as $\varepsilon_{33}^p \neq 0$. The use of $\{\varepsilon^p\}$ instead of $\{\varepsilon^*\}$ as done in

previous finite element analyses (see e.g. Dean and Hutchinson, 1980; Shenoy and Krishna, 1994) is not correct.

Substituting the expression for stresses given in eqn (7) into the weak form of eqn (5) leads to

$$\int_\Omega \delta v_{i,j} C_{ijkl}\varepsilon_{kl}\,\mathrm{d}\Omega - \int_\Omega \delta v_{i,j} C_{ijkl}\varepsilon^p_{kl}\,\mathrm{d}\Omega - \int_\Omega m_s^2 u_{i,1}\delta v_{i,1}\,\mathrm{d}\Omega + \int_\Gamma m_s^2 n_1 u_{i,1}\delta v_i\,\mathrm{d}\Gamma + \int_{\Gamma_t} \delta v_i t_i^*\,\mathrm{d}\Gamma - \int_{\Gamma_u} \delta v_i \lambda_i\,\mathrm{d}\Gamma - \int_{\Gamma_u} \delta\lambda_i (u_i - u_i^*)\,\mathrm{d}\Gamma = 0 \quad (10)$$

Similar to Xu and Saigal (1997a, b), the moving least squares interpolants are used to discretize the displacement vector u and its corresponding test function vector δv as

$$u = \sum_1^n \Phi_I u_I \quad (11)$$

$$\delta v = \sum_1^n \Phi_I \delta v_I \quad (12)$$

where Φ_I is an interpolant generated by the moving least squares method (see Xu, 1996). The Lagrange multipliers and their corresponding test functions are similarly discretized using Lagrange interpolants $\Psi_I(s)$ (see e.g. Xu, 1996; Xu and Saigal, 1997a, b). These discretizations, substituted in the weak form of eqn (10), lead to the discrete system of equations given as

$$\begin{bmatrix} \mathbf{M}-\mathbf{L}+\mathbf{P} & \mathbf{N} \\ \mathbf{N}^T & 0 \end{bmatrix} \begin{Bmatrix} u \\ \lambda \end{Bmatrix} = \begin{Bmatrix} f+f^p \\ q \end{Bmatrix} \quad (13)$$

$$f_I^p = \int_\Omega \mathbf{B}_I^T \mathbf{D}^e \{\varepsilon^*\}\,\mathrm{d}\Omega \quad (14)$$

where the matrices $\mathbf{M}$, $\mathbf{N}$, $\mathbf{L}$, $\mathbf{P}$, $\mathbf{B}_I$ and vectors f, q, are as defined in Xu (1996). f^p is a body force term caused by the plastic strain (see e.g. Dean and Hutchinson, 1980; Parks et al. 1981; Xu and Saigal, 1997b).

Under the condition of small scale yielding (see e.g. Lam and Freund, 1985) a significant zone dominated by the elastic dynamic stress intensity factor K exists around a crack tip. Therefore, the stress or displacement components on the boundary of the domain under consideration should match the dynamic asymptotic stress field or displacement field as long as the boundary is far away from crack tip compared to the maximum extent of the active plastic zone. In addition, the steady state condition implies that the previous elastic–plastic deformation history at a point A (x_1^*, x_2^*) can be traced by the path line $x_2 = x_2^*$ which starts at the point A and is parallel to the direction of the crack growth. In other words, the stress state at the point A can be obtained by integrating the constitutive equations along the path line $x_2 = x_2^*$ starting from the intersection point between the path line and the upstream boundary of the domain under consideration upto the point A. The steady state condition, preferably, requires the use of rectangular elements in the plastic zone in FEM analyses because both the interpolation and integration in FEM rely on elements. As

explained above, the use of rectangular elements in the FEM analyses may result in an ill-conditioned stiffness matrix.

3. Constitutive equations

In the present study, both rate-independent and rate-dependent constitutive equations are considered. For rate-independent materials, strain hardening is also considered.

3.1. *Rate-independent stress–strain relationships*

Two type of strain hardening stress–strain relationships were employed (see e.g. Xu, 1996). The linear hardening relation in shear is given as

$$r-1=\alpha(\gamma-1) \tag{15}$$

where $\alpha=\mu_t/\mu$ is the local slope of the non-dimensional stress–strain curve in pure shear. The power-law hardening relation in shear is given as

$$\tau=\gamma^{\mathrm{n}} \tag{16}$$

where n is the hardening exponent.

The elastic–perfectly plastic case can be deduced from the above hardening stress–strain relationships: for $\alpha=0$, the linear strain hardening stress–strain relationship reduces to the elastic–perfectly plastic case; for $n=0$, the power hardening stress–strain relationship also reduces to the elastic–perfectly plastic case.

3.2. *Rate-dependent stress–strain relationships*

The material elements in close proximity to the crack tip running at a high speed experience a very large strain-rate, which is usually above $10^3\ \mathrm{s}^{-1}$ (see e.g. Freund and Hutchinson, 1985; Mataga, 1986). For most visco-plastic materials, the material response shows a dramatic increase in flow resistance at strain-rates above the transition strain-rate $\dot{\bar{\gamma}}_t$ (about 10^3 or $10^4\ \mathrm{s}^{-1}$). To describe this feature of visco-plastic materials, an idealized visco-plastic response was employed by Freund and Hutchinson (1985) and Mataga et al. (1987) and is also used here. In the idealized viscoplastic constitutive equations: at low strain-rates (plastic shear strain-rate $\dot{\bar{\gamma}}^p \leqslant \dot{\bar{\gamma}}_t$), the material is assumed to be elastic–perfectly plastic with $\bar{\tau}=\tau_y$; at high strain-rates, the increase of the plastic shear strain-rate is linearly proportional to the increase of stress as

$$\dot{\bar{\gamma}}^p=\dot{\bar{\gamma}}_t+\frac{\dot{\bar{\gamma}}_0(\bar{\tau}-\tau_y)}{\mu} \quad \bar{\tau}>\tau_y \tag{17}$$

In a non-dimensional form, the constitutive model is expressed as

$$\tau=1 \quad \dot{\gamma}^p \leqslant Q\xi \tag{18}$$

$$\dot{\gamma}^p=Q\xi+Q(\tau-1) \quad \dot{\gamma}^p>Q\xi \tag{19}$$

where $\dot{\gamma}^p=\dot{\bar{\gamma}}^p/t_c$ is the non-dimensional shear plastic strain-rate; $t_c=l/c_2$ is the characteristic time;

$\xi = \mu\dot{\bar{\gamma}}_t/\tau_y\dot{\bar{\gamma}}_0$ is a non-dimensional combination of the material parameters; and $Q = \mu\dot{\bar{\gamma}}_0 G/c_2\tau_y^2$ is a non-dimensional combination of the material parameters and the overall driving force, and is termed in the present study as the material-loading parameter.

3.3. *Multi-axial stress–strain relationships*

The material behavior is assumed to be characterized by von Mises yielding condition and an associated flow rule. The strain hardening is assumed to be isotropic. The total non-dimensional strain-rate is given as $\dot{\varepsilon}_{ij} = \dot{\varepsilon}^e_{ij} + \dot{\varepsilon}^p_{ij}$, where the non-dimensional elastic strain-rate can be expressed as

$$\dot{\varepsilon}^e_{ij} = \frac{1}{2(1+\nu)}[(1+\nu)\dot{\sigma}_{ij} - \nu\dot{\sigma}_{kk}\delta_{ij}] \tag{20}$$

The non-dimensional plastic strain-rate can be expressed for both rate-independent and rate-dependent materials as

$$\dot{\varepsilon}^p_{ij} = \frac{\dot{\lambda}s_{ij}}{2\tau} \tag{21}$$

where s_{ij} is the non-dimensional stress deviator, $\dot{\lambda}$ represents a non-dimensional effective plastic shear strain-rate, and is given as

$$\dot{\lambda} = \begin{cases} \left(\dfrac{1}{\alpha} - 1\right)\dot{\tau} & \text{for linear hardening} \\ \left(\dfrac{1}{n}\tau^{(1/n)-1} - 1\right)\dot{\tau} & \text{for power hardening} \end{cases} \tag{22}$$

for non-hardening, elastic–perfectly plastic materials

$$\tau = 1 \tag{23}$$

for rate-dependent materials

$$\tau = 1 \quad \dot{\gamma}^p \leqslant Q\xi \tag{24}$$

$$\dot{\gamma} = Q\xi + Q(\tau - 1) \quad \dot{\gamma}^p > Q\xi \tag{25}$$

4. Integration of constitutive equations

The key step in the iterative scheme for solving the non-linear system of eqns (13) is the calculation of the body force term $\int \mathbf{B}_I^T \mathbf{D}^e \{\varepsilon^*\}\, d\Omega$. To compute this term, the plastic strains are used at each integration point which are obtained from the stresses at that point. Further, the previous stress and deformation histories of the material point are required so as to obtain the stress state at the point. As mentioned above, the steady state condition indicates that the stress state at a point (x_1^*, x_2^*) can be reached by integrating the constitutive equation along the path line

$x_2 = x_2^*$ starting from the intersection point between the path line and the upstream boundary of the domain under consideration upto the point (x_1^*, x_2^*).

In order to satisfy the implicit steady state condition and to take advantage of it, the body force term f^p was determined by computing the contributions to the integral, $\int \mathbf{B}_I^T \mathbf{D}^e \{\varepsilon^*\}\, d\Omega$, layer by layer. Each layer is divided into a certain number of cells each of the same height as that of the layer. These cells correspond to the EFG cells in the present study. The integration in each layer is computed cell by cell from right to left. For each cell, the same number of integration points are employed. The integration of the constitutive equations is performed along two adjacent integration points at the same height. Assuming that the stress state at the left integration point is known, the strain increment is approximated by the difference between the strains at two adjacent integration points. Further, assuming that the strain-rate during this small step stays constant, the scheme developed by Mataga (1986) can be used to perform the integration of the constitutive equations.

The EFG method affords two distinct advantages (see e.g. Xu, 1996 and the references listed therein). First, the integration scheme described above preferably requires rectangular elements with the same height as that of a layer in which they occur for a FEM analysis. Refining a mesh at the crack tip leads to the need for a large number of layers. The separation of the interpolation scheme and the domain integration in the EFG method overcomes this problem. Second, more integration points can be used in any cell to achieve the desired accuracy. These two features lead to better accuracies of solutions obtained using the EFG method compared to the FEM.

5. Solution strategy

Since the body force term, f^p, is also a function of the unknown displacement vector u, the system of eqns (13) is nonlinear and requires an iterative scheme for its solution. The iterative algorithm proposed by Dean and Hutchinson (1980), Parks et al. (1981) and Lam and Freund (1985) was implemented in the present study. The iterative procedure starts with an initial estimate of the solution and a trial displacement field is obtained from the system of eqns (13). Using these displacements, the strain field is next computed. Based on the constitutive equation integration algorithm, the stress and plastic strain components can be obtained at each integration point of the domain Ω. The body force term, f^p, due to the plastic strain is then computed using eqn (14). The above procedure is repeated until a convergent displacement field is reached.

During each iteration, the matrices **M**, **N**, **L** and **P** remain unchanged. Furthermore, the matrices **M**, **N**, **L** and **P** depend only upon the arrangement of nodal points in the domain under consideration and the crack speed m_s. Constitutive equations influence only the right hand side vector f^p. Thus, the stiffness matrix of eqn (13) is needed to be constructed and decomposed only once for all steady dynamic crack growth problems for various materials. For a given crack speed, m_s, numerical solutions were obtained for a series of steady dynamic crack growth problems. The elastic solution ($\{\varepsilon^*\} = 0$) was employed as an initial estimate of the solution to the first problem. Then, the solution to the previous problem was employed as the initial estimate of the solution to the subsequent problem.

6. Numerical results and discussions

Due to the symmetry of mode I cracks, only the upper half of the domain under consideration was considered. Two different nodal point arrangements and the corresponding Lagrange mul-

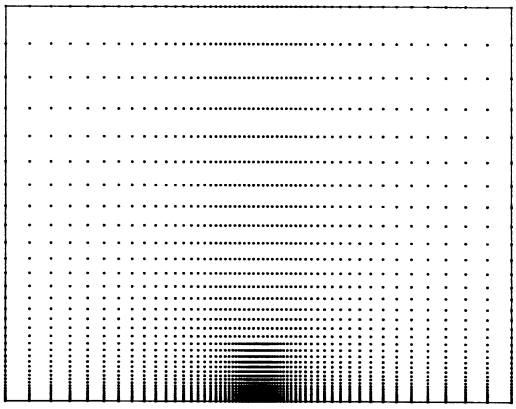

(a)

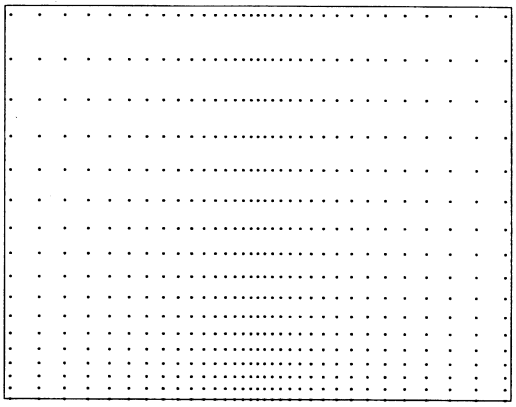

(b)

Fig. 2. Arrangements of 2127 nodal points: (a) global arrangement and (b) local refined arrangement near the tip.

tipliers: 2127 nodal points shown in Fig. 2 with 35 Lagrange multipliers, and 2925 nodal points shown in Fig. 3 with 41 Lagrange multipliers, respectively, were employed. Linear basis functions were used to generate the moving least squares interpolants. A total of 2312 and 3200 domain integration cells were used for the arrangement of 2127 points and that of 2925 points, respectively. A 5×5 numerical integration scheme was employed in each integration cell. The overall size of the domain under consideration is about 20 times the maximum extent of the active plastic zone. The following boundary conditions were imposed in the numerical analyses (see e.g. Xu, 1996). The crack surface was considered to be traction free and the normal displacements on the remainder of the crack plane edge were constrained to be zero. Tractions were applied to the other three sides of the domain under consideration according to the asymptotic elastic stress field given by Freund

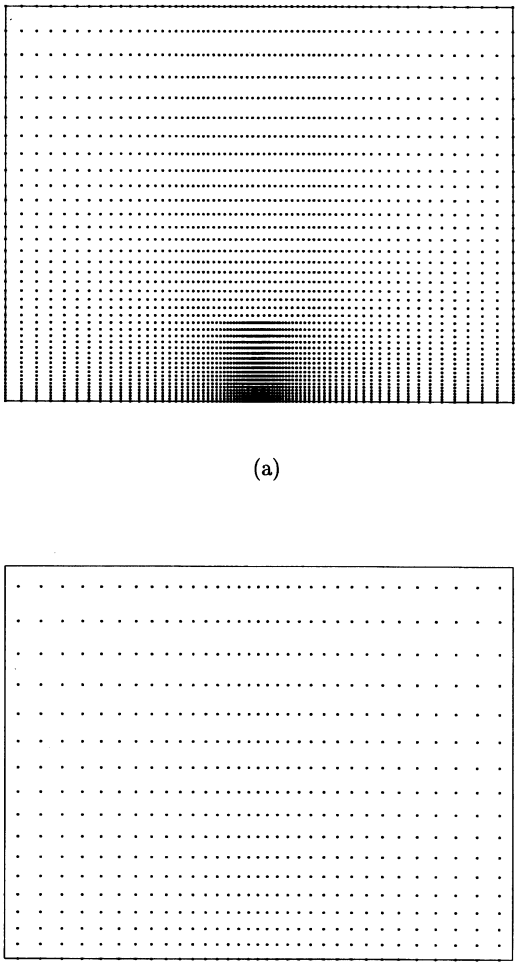

Fig. 3. Arrangements of 2925 nodal points: (a) global arrangement and (b) local refined arrangement near the tip.

(1976). As stated earlier, the asymptotic elastic stress field has the same singular form as given in eqn (1) except for using the remote elastic dynamic stress intensity factor K instead of the near-tip stress intensity factor K_{tip}. Similarly, K is related to the remote energy release rate G as given in eqn (2) with K and G replacing K_{tip} and G_{tip}, respectively.

The existence of the plastic wake will cause a mismatch between the tractions imposed according to the asymptotic elastic stress field and the numerical solution in the wake. As reported by Mataga (1986), this mismatch has only a slight influence on the near-tip numerical solution as long as the overall size of the domain under consideration is large enough compared to the maximum extent of the active plastic zone. Based on these arguments, the influence of the mismatch on the near-tip numerical solution can be ignored for the present study.

In all numerical analyses reported here, a Poisson's ratio of 0.3 for both rate-independent materials and rate-dependent materials was used. For rate-dependent materials, $Q = 50, 35, 20, 5$ and $\xi = 0.1, 0.01$ were adopted to investigate the influence of the viscous material parameters. Using the present arrangement of nodal points, numerical solutions based on EFG formulations exhibited divergence for non-dimensional crack speeds m_s greater than 0.6. The convergence criterion employed in the present study is given as $|(u_i^{(n)} - u_i^{(n-1)})/u_i^{(n)}| \leqslant \mathrm{DTOL}$, where $u_i^{(n)}$ is a component of the solution displacement vector at the nth iteration. A maximum tolerance DTOL of 0.025 was employed. In most cases, 10–40 iterations were needed to obtain the solution to the problem of steady dynamic crack growth in rate-independent materials; and 5–20 iterations were needed to obtain the solution to the problem of steady dynamic crack growth in rate-dependent materials.

The numerical results for steady dynamic crack growth in rate-independent materials are presented first with emphasis on the influence of crack speeds and of strain hardening of materials. For the influence of crack speeds, the numerical results presented in this paper confirmed the observations made in previous studies (see e.g. Achenbach and Dunayevsky, 1981b; Lam and Freund, 1983, 1985). As for the influence of strain hardening of materials, the numerical results presented here for the first time revealed the trend of this influence on the mechanics of steady dynamic crack growth. The numerical results for steady dynamic crack growth in rate-dependent materials are presented next with emphasis on determining the relationship between G_{tip} and G. These results further demonstrated the validity of the assumptions made in the literature in deriving the closed form relations for G_{tip} and G by Freund and Hutchinson (1985) and Mataga et al. (1987). Also, a comparison of the relationship between G_{tip} and G obtained from analytical and numerical results, respectively, was made.

6.1. *Steady dynamic crack growth in non-hardening materials*

(1) Near-tip stress distributions

Steady cracks moving at a non-dimensional speed of $m_s = 0.05$ were considered. The angular distributions of stresses at the non-dimensional radial distances $r = 0.015$ and 0.03, which are normalized by the characteristic length l, are shown in Fig. 4 for $m_s = 0.05$. The asymptotic stress distributions due to Achenbach and Dunayevsky (1981b) which are applicable only to low crack speeds are also shown in this figure for comparison. As seen from this figure, the stress distributions for σ_{11} and σ_{12} at various radial distances are nearly the same and are in good agreement with the asymptotic ones. However, the computed stress distributions for σ_{22} can not clearly reveal the same independence with respect to the radial distance. The differences may be attributed to the difference between the material model used in the present study and the material model used by Achenbach and Dunayevsky (1981b). As stated earlier, the Tresca yielding condition and the Mises flow rule were used in the asymptotic analysis presented by Achenbach and Dunayevsky (1981b), while the Mises yielding condition and the associated flow rule were employed in the present study.

A comparison between the present study and the FEM analyses presented by Lam and Freund (1985) is shown in Fig. 5(a) for stress distributions at the non-dimensional radial distance $r = 0.0142$ that is normalized by the characteristic length l for $m_s = 0.4$, noting that $r = 0.0142$ in the

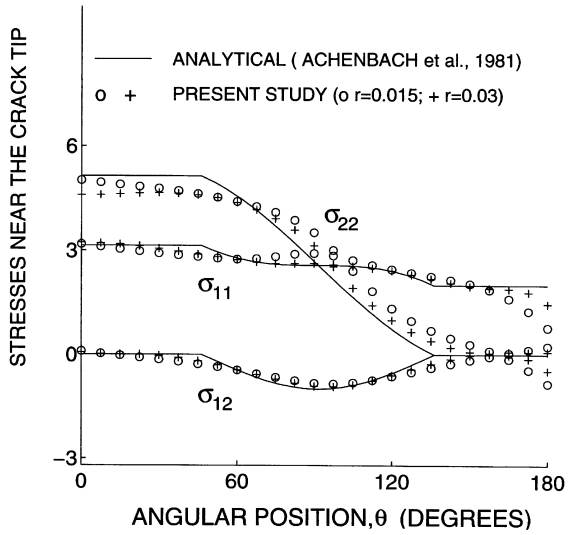

Fig. 4. Stresses around the moving crack tip in an elastic–perfectly plastic material with crack speed $m_s = 0.05$.

present study is equivalent to $0.017(K/\sigma_0)^2$ used by Lam and Freund (1985). As seen from Fig. 5(a), the two numerical analyses reveal the same trend and are in good agreement. The stress fields near the tip growing steadily in an elastic perfectly–plastic material, as shown in Fig. 5(b), have similar angular distribution patterns for various crack speeds. The influence of crack speeds on the computed near-tip stress fields is shown in Fig. 5(b). A sector of uniform stress field exists ahead of the moving crack tip. With increasing crack speeds, for example from $m_s = 0.1$ to $m_s = 0.4$, this sector becomes more apparent and the stress components σ_{11} and σ_{22} in this sector reduce remarkably as was also observed by Lam and Freund (1985).

(2) Active plastic zones

The active plastic zones near the moving crack tip were obtained for $m_s = 0.1$, 0.2, 0.3 and 0.4 and are shown in Figs 6(a)–6(d), respectively, with the blank portion representing the active plastic zones. The points shown in these figures represent the integration points at which the stress state is elastic. The maximum vertical extent of the active plastic zone increases with increasing crack speeds as also reported by Lam and Freund (1985). Compared to the plastic zones for various crack speeds given by Lam and Freund (1983), the following trends were observed by both Lam and Freund (1983) and the present study: the elastic unloading zone increases in size with increasing crack speeds; the plastic reloading zone is located farther away from the crack tip for large crack speeds, such as $m_s = 0.4$. However, the differences in the active plastic zone shapes for various crack speeds shown in Lam and Freund (1983) could not be observed in the present study.

The existence of the elastic unloading zone behind the moving crack tip was not reported by Slepyan (1976) and Achenbach and Dunayevsky (1981b) for steady dynamic crack growth in compressible materials, and by Gao and Nemat-Nasser (1983) and Leighton et al. (1987) for steady dynamic crack growth in incompressible materials. All of these asymptotic solutions ruled out the elastic unloading sector from the near-tip fields for all crack speeds. The existence of the

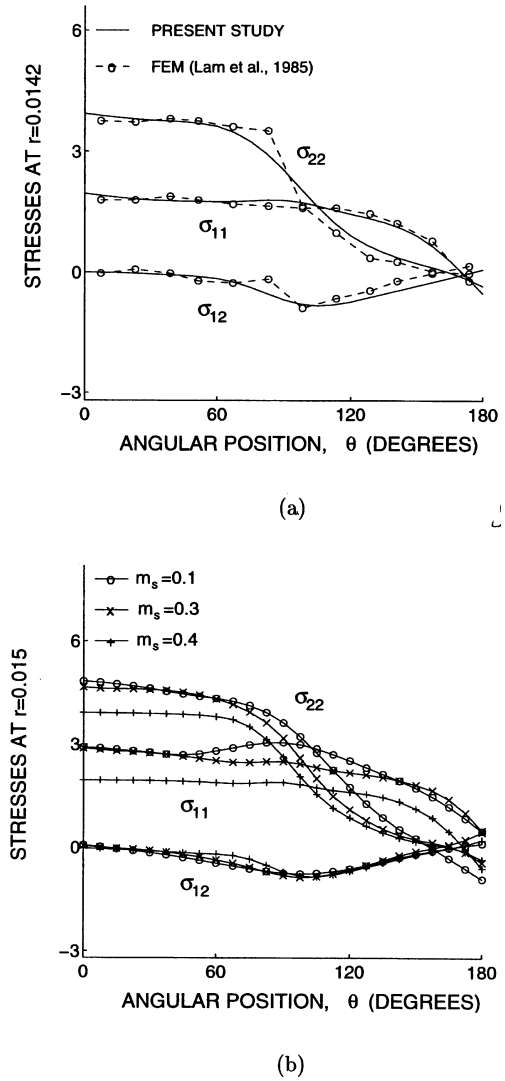

Fig. 5. (a) Stresses around the moving crack tip in an elastic–perfectly plastic material with a crack speed $m_s = 0.4$; (b) influence of crack speeds on stress distributions in an elastic–perfectly plastic material.

elastic unloading zone behind the moving crack tip appears in our numerical results and in the results reported by Lam and Freund (1985). A further study is required to establish the range of validity of the asymptotic solutions.

(3) Crack opening profiles and theoretical fracture toughnesses

The crack opening profiles were obtained for various crack speeds of $m_s = 0.1$, 0.3 and 0.4 for steady dynamic crack growth in an elastic perfectly-plastic material and are shown in Fig. 7. It is noted that the non-dimensional crack opening displacement is given by $\delta = 2u_1(x_1, 0)$. Using these

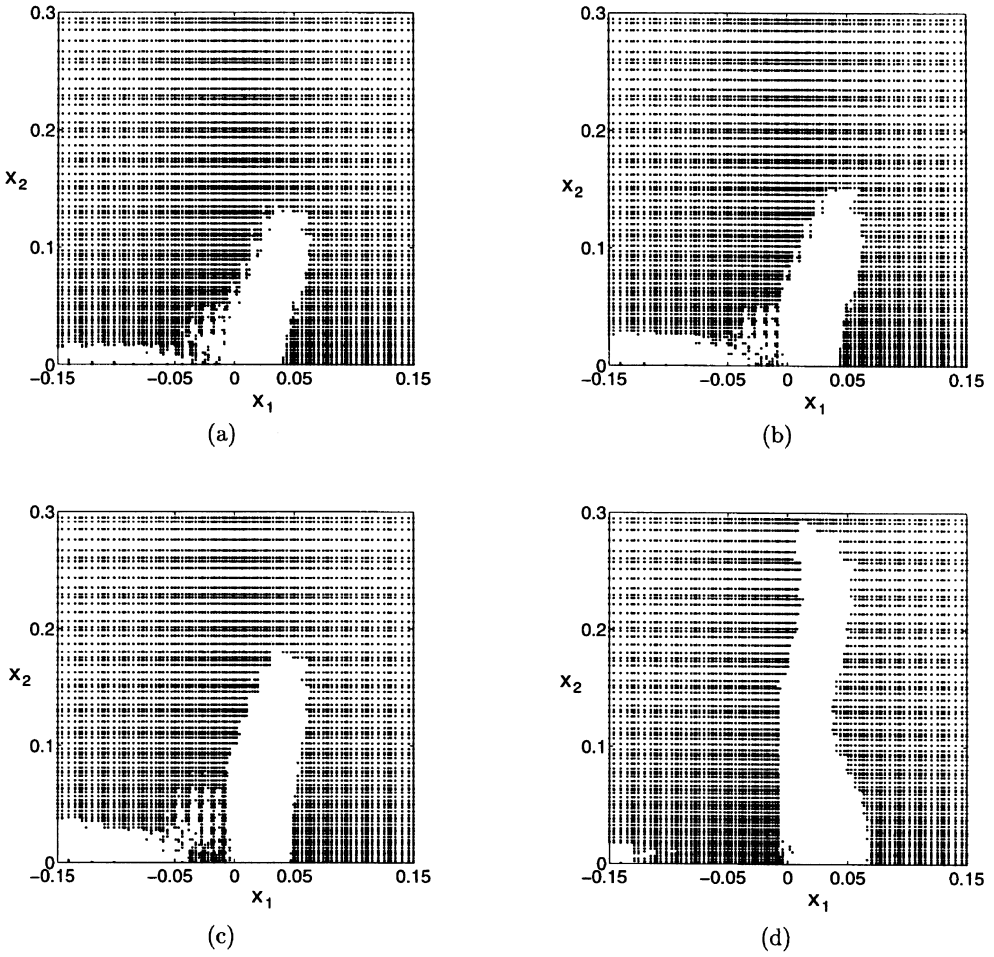

Fig. 6. Active plastic zones in elastic–perfectly plastic materials with non-dimensional crack speeds of (a) $m_s = 0.1$; (b) $m_s = 0.2$; (c) $m_s = 0.3$; and (d) $m_s = 0.4$.

non-dimensional computed crack opening profiles, the effect of crack speeds on the relationship between theoretical fracture toughness and crack face opening angle, $\delta/r = \mu\bar{\delta}/\tau_y\bar{r}$, as shown in Fig. 8, may be obtained. To construct this relationship, it is assumed that the same fracture criterion is applicable for the steady growth of a moving crack as is used for the initiation of a stationary crack (see e.g. Dean and Hutchinson, 1980; Lam and Freund, 1985). The fracture criterion based on crack opening displacements is adopted here. According to this criterion, a stationary crack initiates as the crack opening displacement $\bar{\delta}$ at $\bar{r} = \bar{r}_c$ reaches a critical value $\bar{\delta}_c$ under a remote driving force (energy release-rate) G_c. Correspondingly, once the steady state of crack growth has been established, the crack keeps running at a constant speed after the crack opening displacement $\bar{\delta}$ at $\bar{r} = \bar{r}_c$ (measured from the moving crack tip) reaches a critical value $\bar{\delta}_c$ under a remote driving force G_d. The ratio G_d/G_c may be obtained based on the crack opening profiles for moving cracks given in Fig. 7 and those for a stationary crack given by Tracey (1976).

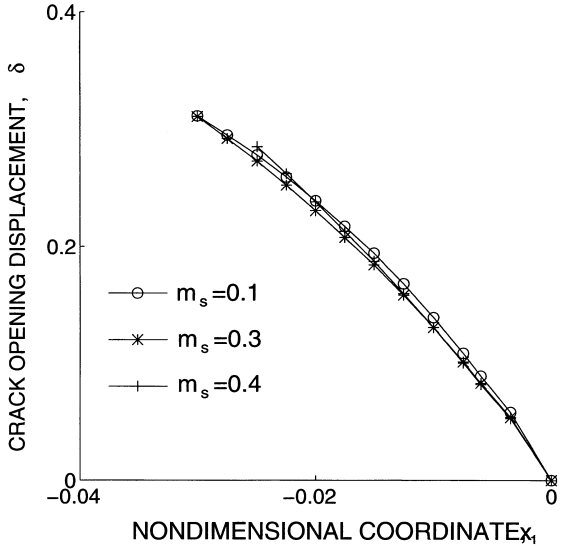

Fig. 7. Crack opening profiles for an elastic–perfectly plastic material for various crack speeds.

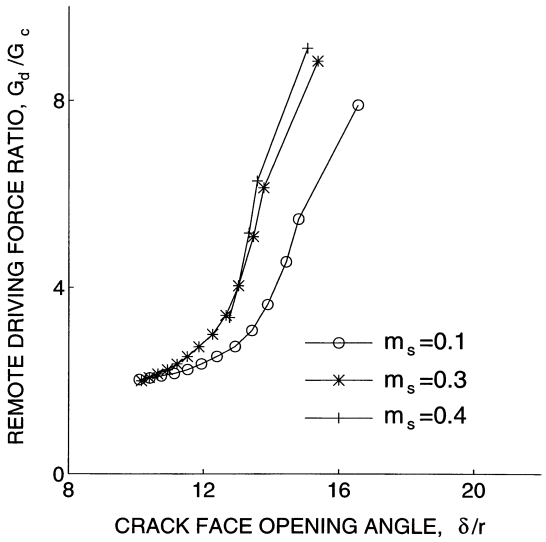

Fig. 8. The influence of crack speeds on the relationship between the remote driving force G_d/G_c and the crack face opening angle.

The variation of remote driving force, G_d/G_c, with the crack face opening angle, δ/r, that is required to propagate the crack steadily is shown in Fig. 8 for crack speeds of $m_s = 0.1$, 0.3 and 0.4. From this figure, it is seen that G_d/G_c increases as m_s increases for a given crack face opening angle. Thus, a larger dynamic driving force G_d/G_c is needed to keep a crack running at a faster speed. The same trend was also observed by Lam and Freund (1985).

6.2. *Steady dynamic crack growth in hardening materials*

In this section, the influence of strain hardening on various features of steady dynamic crack growth is studied. Results on this topic have not been reported in the literature to date.

To investigate the effect of strain hardening, the comparisons of solutions corresponding to various hardening levels and all for the same crack speed are made. The influence of strain hardening was observed through numerous numerical studies to have the same trend for various speeds. The numerical solutions for a crack speed of $m_s = 0.3$ were used to illustrate the effect of strain hardening in this study.

(1) Near-tip stress distributions

The near-tip angular distributions of stresses at non-dimensional radial distances $r = 0.015$ and 0.03 are shown in Figs 9(a) and (b) for the power hardening material with $n = 0.2$ and for the linear hardening material with $\alpha = 0.1$, respectively. The common features of the stress distributions shown in Fig. 9 is that the magnitudes of σ_{11} and σ_{22} increase remarkably with decreasing radial distance r, especially in the zone ahead of the moving crack tip. A similar trend has also been observed for steady, quasi-static moving cracks (see e.g. Xu and Saigal, 1997b).

The angular distributions of stresses at the non-dimensional radial distance $r = 0.015$ are shown in Fig. 10(a) for power hardening materials with $n = 0.2$, 0.1 and 0.0 and in Fig. 10(b) for linear hardening materials with $\alpha = 0.1$, 0.05 and 0.0, respectively. The effect of strain hardening on the near-tip stress field can be seen from these figures. With increasing strain hardening, the amplitudes of the stresses increase except in the portion near the crack flank. This trend exists for both power hardening materials and linear hardening materials. A similar phenomenon was also observed for steady, quasi-static moving cracks (see e.g. Xu and Saigal, 1997b).

(2) Active plastic zones

The active plastic zones surrounding the moving crack tip are shown in Figs 11(a)–(d): for the power hardening materials in Figs 11(a) and (b) for $n = 0.2$ and $n = 0.1$, respectively; and for the linear hardening materials in Figs 11(c) and (d) for $\alpha = 0.1$ and $\alpha = 0.05$, respectively. The general characteristics of the active plastic zones shown in Fig. 9 are the same. A large active plastic zone surrounding the moving crack tip as well as a plastic reloading zone are observed. An elastic unloading sector lying between these two zones can also be observed.

The height of the plastic reloading zone increases with decreasing strain hardening for both power hardening and linear hardening materials. Accordingly, with this increase, the elastic unloading sector also becomes apparent. With decreasing strain hardening, the maximum non-dimensional vertical extent, h, of the active plastic zone increases. For power hardening materials, h increases from 0.162–0.173 as n decreases from 0.2–0.1; for linear hardening materials, h increases from 0.163–0.173 as α decreases from 0.1–0.05.

(3) Crack opening profiles and theoretical fracture toughnesses

The crack opening profiles for power hardening materials with $n = 0.2$, 0.1 and 0.0 were obtained for a crack speed of $m_s = 0.3$ and are shown in Fig. 12. Based on these crack opening profiles, the influence of strain hardening on the relationship between the non-dimensional remote driving force, G_d/G_c, and the crack face opening angle, δ/r, may be investigated. Using the same crack

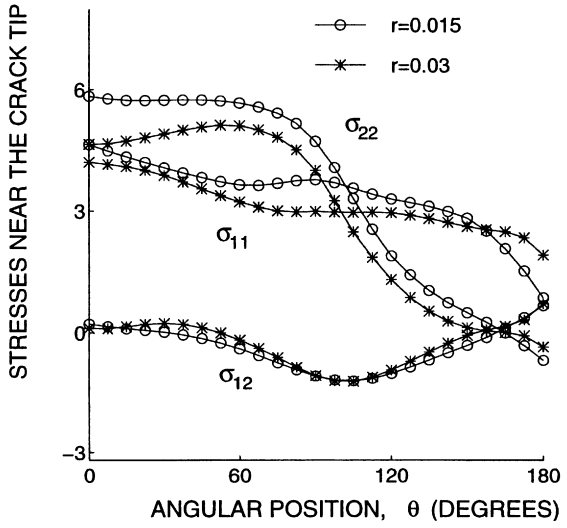

(a)

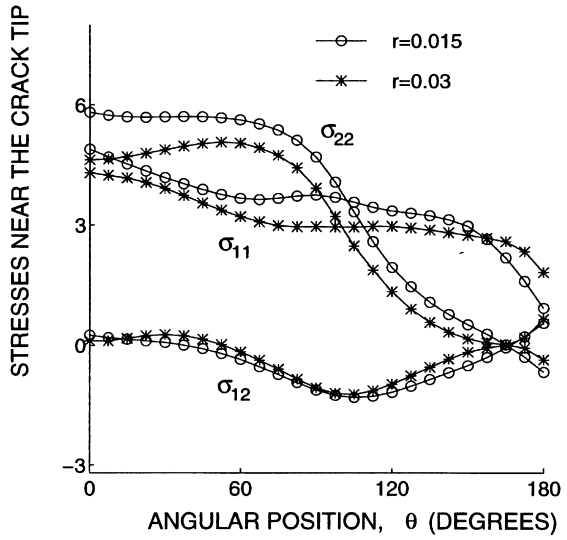

(b)

Fig. 9. Variation of stresses with the radial distance r in hardening materials: (a) power hardening materials with $n = 0.2$; and (b) linear hardening materials with $\alpha = 0.1$.

opening displacement based fracture criterion as mentioned above for elastic–perfectly plastic materials, and assuming that this criterion can be applied to both crack initiation and crack growth in the same material, the relationships for the non-dimensional remote driving force, G_d/G_c, vs the crack face opening angle δ/r, were obtained for strain hardening parameters $n = 0.2$, 0.1, and 0.0,

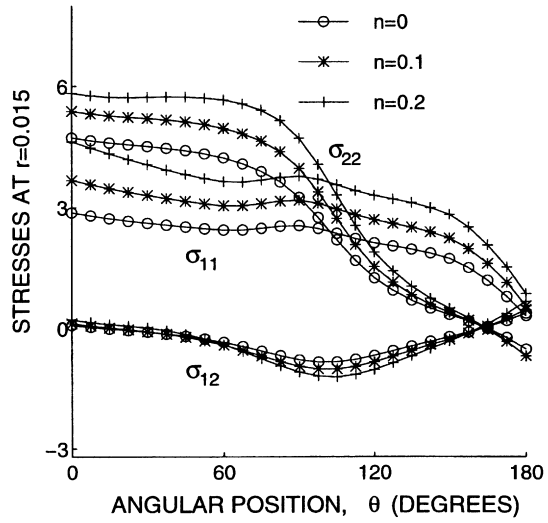

(a)

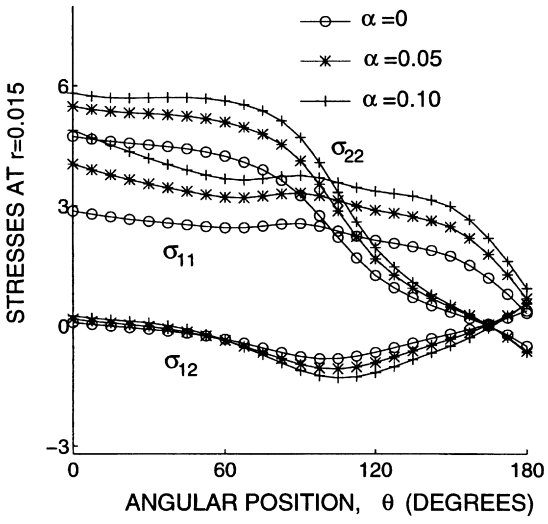

(b)

Fig. 10. The influence of strain hardening on the near-tip angular stress distribution at $r = 0.015$: (a) power hardening materials; and (b) linear hardening materials.

respectively, and are shown in Fig. 13. Similar to the trend observed by Dean and Hutchinson (1980), Lam and Freund (1985) and Xu and Saigal (1997b) for steady, quasi-static moving cracks, the non-dimensional remote driving force, G_d/G_c, increases with decreasing strain hardening. This

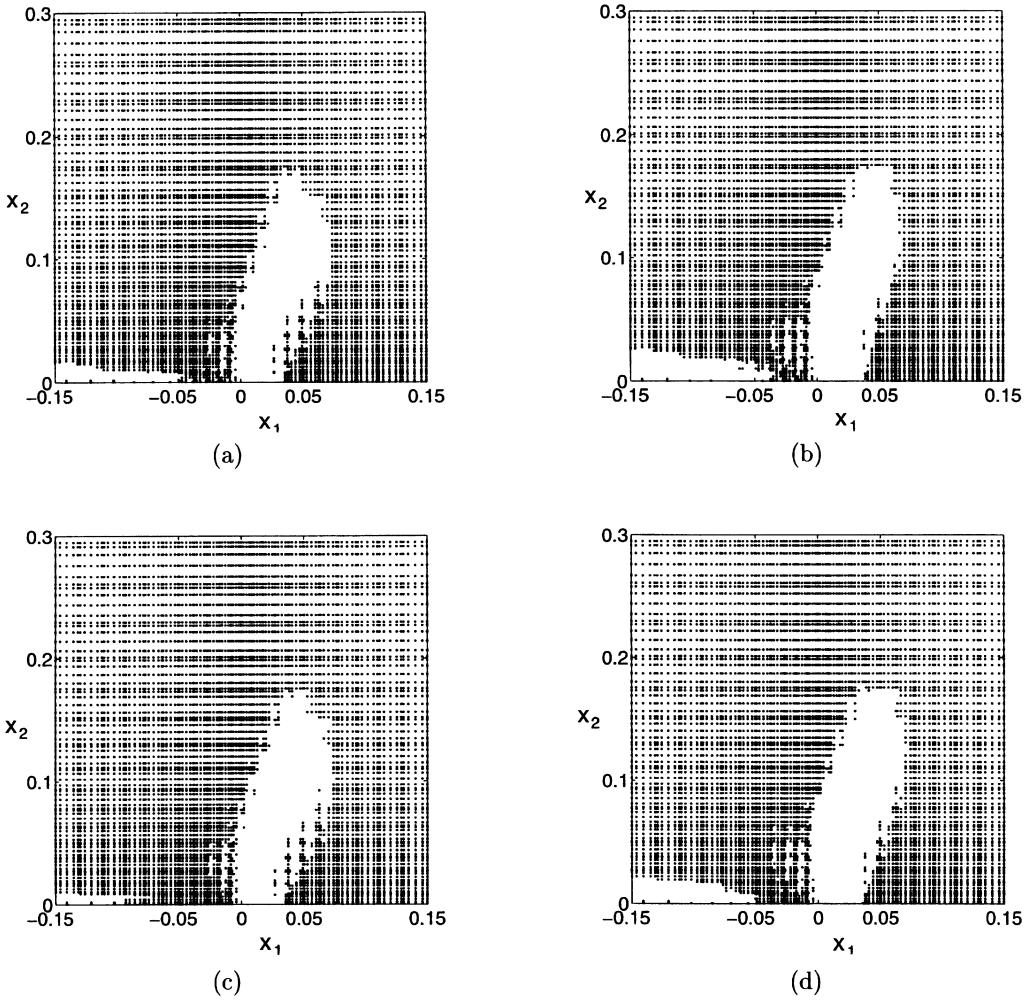

Fig. 11. Active plastic zones for hardening materials with crack speed $m_s = 0.3$: (a) power hardening, $n = 0.2$; (b) power hardening, $n = 0.1$; (c) linear hardening, $\alpha = 0.1$; and (d) linear hardening $\alpha = 0.05$.

trend indicates that materials with lower hardening provide greater resistance to steady dynamic crack growth.

6.3. *Steady dynamic crack growth in viscoplastic materials*

Numerical calculations based on the EFG formulation presented in this study have been performed for a variety of combinations of material parameters and crack speeds. In this section, the numerical solutions are presented and their comparisons against the asymptotic solutions are made. A brief review of the analytical solutions presented by Freund and Hutchinson (1985) and Mataga et al. (1987) is given in the Appendix.

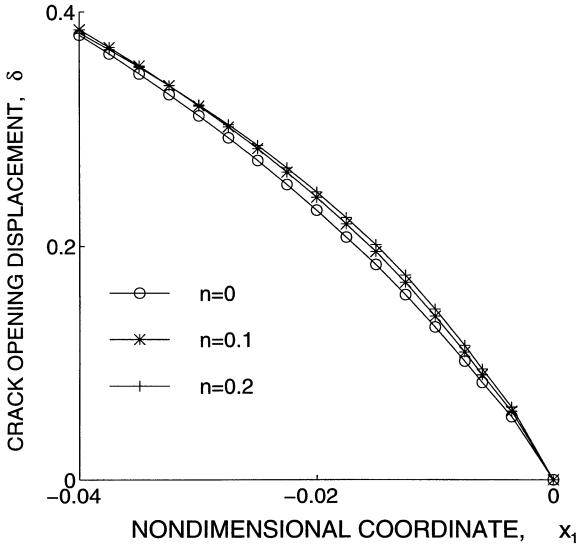

Fig. 12. The influence of strain hardening on crack opening profiles for crack speed $m_s = 0.3$ for power hardening materials.

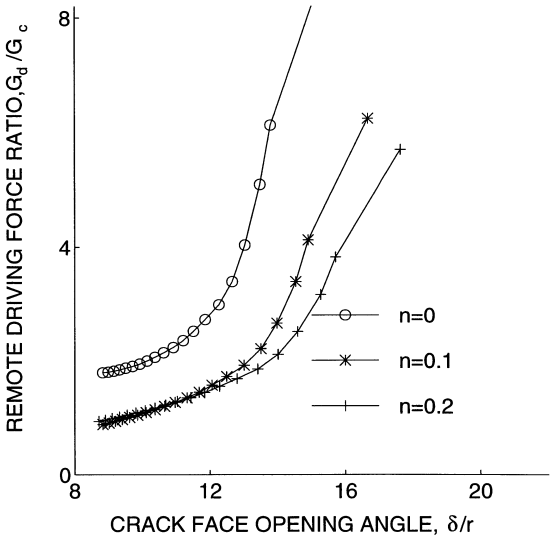

Fig. 13. The influence of strain hardening on the relationship between the remote driving force G_d/G_c and the crack face opening angle for crack speed $m_s = 0.3$.

(1) Near-tip angular stress distributions

The near-tip angular stress distributions for $m_s = 0.2$ and 0.4, $Q = 5$, and $\xi = 0.1$ are used to examine the characteristics of the stress field near the tip of high strain-rate cracks. The near-tip angular stress distributions for $m_s = 0.2$ at non-dimensional radial distances $r = 0.015$ and $r = 0.03$

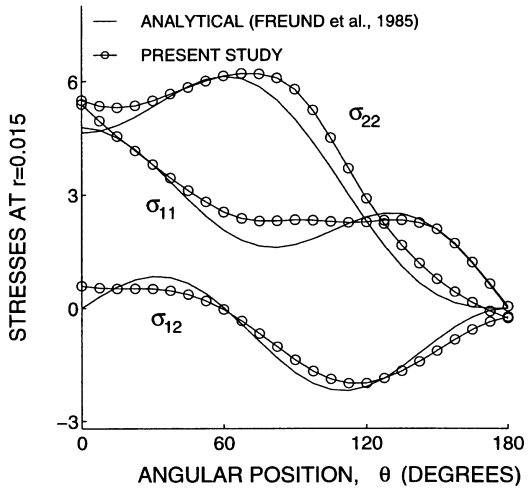

(a)

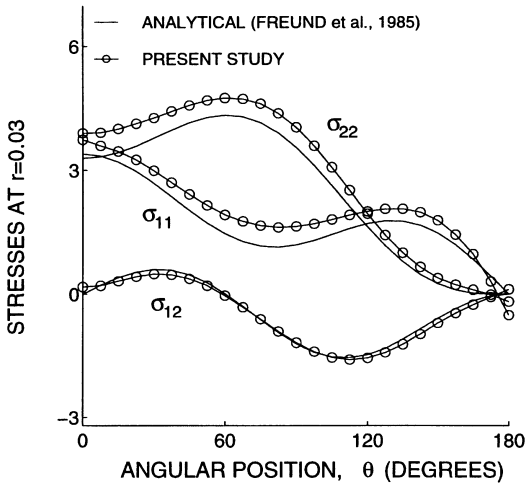

(b)

Fig. 14. The near-tip stresses for high strain-rate cracks for $m_s = 0.2$, $Q = 5$ and $\xi = 0.1$ at radial distances: (a) $r = 0.015$; and (b) $r = 0.03$.

are shown in Figs 14(a) and (b), respectively. The corresponding stress distributions for $m_s = 0.4$ are shown in Figs 15(a) and (b), respectively. The analytical results in these figures correspond to the near-tip stress field given in eqn (1). The near-tip stress intensity factor K_{tip} is determined according to eqn (2) from the computed value of G_{tip}/G. The values of G_{tip}/G were taken to be 0.7347 and 0.8334, which were first obtained by calculating a path independent integral and will

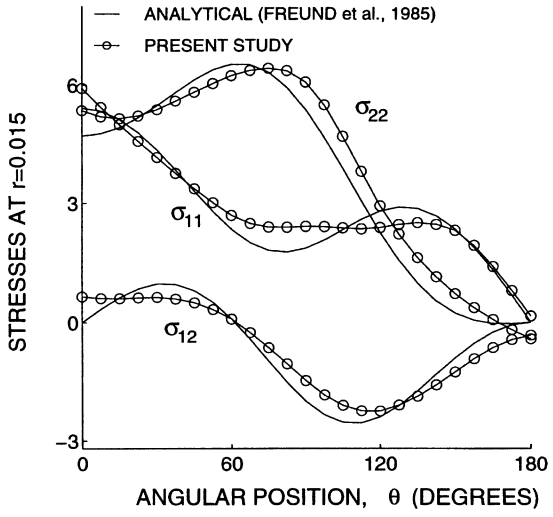

(a)

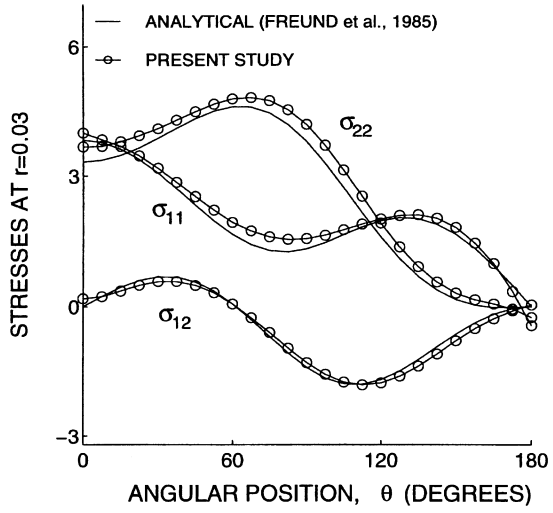

(b)

Fig. 15. The near-tip stresses for high strain-rate cracks for $m_s = 0.4$, $Q = 5$ and $\xi = 0.1$ at radial distances: (a) $r = 0.015$; and (b) $r = 0.03$.

be discussed later, for $m_s = 0.2$ and 0.4, respectively. Good agreements of the computed near-tip angular stress distributions with the analytical results are seen for both radial distances in these figures. These agreements indicate that using the stress field given by the relation in eqn (1) in the entire active plastic zone (see Freund and Hutchinson, 1985) is a good simplification for this case.

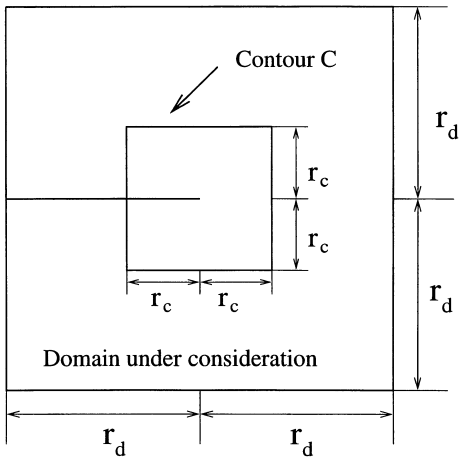

Fig. 16. The integral contour C used to calculate the crack-tip energy release rate G_{tip}/G. r_d is the size of the domain under consideration.

(2) Path independence of crack-tip energy release-rate G_{tip}/G

The crack-tip energy release-rate G_{tip}/G may be expressed using a path independent integral as

$$\frac{G_{tip}}{G} = \int_C [(U+T)n_1 - \sigma_{ij} n_j u_{i,1}] \, d\Gamma \tag{26}$$

where U is the non-dimensional stress work density; $T = \frac{1}{2} m_s^2 u_{i,1} u_{i,1}$ is the non-dimensional kinetic energy density; C is an arbitrary contour described in a counterclockwise fashion; and n_j is the jth component of the normal to the contour C.

The contour integral was computed along the contour C shown in Fig. 16, and values of r_c were taken to be 0.02, 0.04, 0.06, 0.08, 0.10, 0.12, 0.16, 0.20 and 0.24, respectively. A typical variation of the computed G_{tip}/G with respect to the size r_c of integral contours is shown in Fig. 17. A good independence of the computed G_{tip}/G with respect to integral contours is observed from this figure. The average values of G_{tip}/G over $0.02 \leqslant r_c \leqslant 0.12$ and maximum differences from the average value for various combinations of m_s, ξ and Q, were computed corresponding to these paths and are given in Table 1. It is seen from this table that the maximum difference between the values of G_{tip}/G computed using these paths and the average value of G_{tip}/G is 2.45% and corresponds to $r_c = 0.02$. For most paths, this difference is below 0.5%. These discrepancies of G_{tip}/G for various paths used for the evaluation of the line integral are smaller than those reported by Freund and Hutchinson (1985) and Ostlund (1990) and are reasonable for a numerical study to indicate path independence. This path independence provides a further validation of the procedures of this study. The average value of G_{tip}/G from these integration paths was employed for all subsequent calculations.

(3) Active plastic zones

The active plastic zone in viscoplastic materials is composed of two zones: a high strain-rate zone, and a low strain-rate zone. As typical illustrations, the low and high strain-rate zones for a

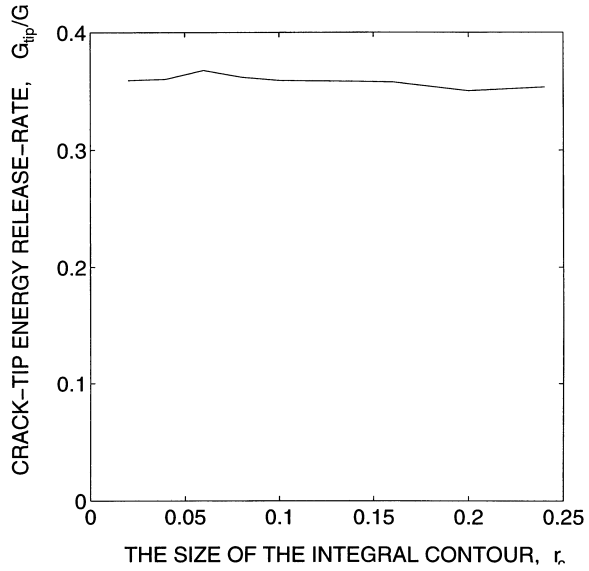

Fig. 17. The variation of computed crack-tip energy release-rate G_{tip}/G with respect to the size r_c of integral contours for $m_s = 0.4$, $Q = 50$ and $\xi = 0.1$.

Table 1
Path independence of G_{tip}/G

Case	Q	Maximum relative error (%)	Averaged G_{tip}
A	50	2.45	0.2675
	35	1.73	0.3352
	20	1.51	0.4505
	5	1.06	0.7347
B	50	1.71	0.3619
	35	1.37	0.4447
	20	0.98	0.5782
	5	0.69	0.8334
C	50	1.39	0.3943
	35	1.17	0.4797
	20	0.92	0.6123
	5	0.66	0.8509

Case A: $m_s = 0.2$, $\xi = 0.1$. Case B: $m_s = 0.4$, $\xi = 0.1$. Case C: $m_s = 0.4$, $\xi = 0.01$.

crack speed of $m_s = 0.3$, the material parameter $\xi = 0.1$, and for two different values of material-loading parameters, $Q = 50$ and 10, are shown in Figs 18 and 19, respectively. The parameter Q

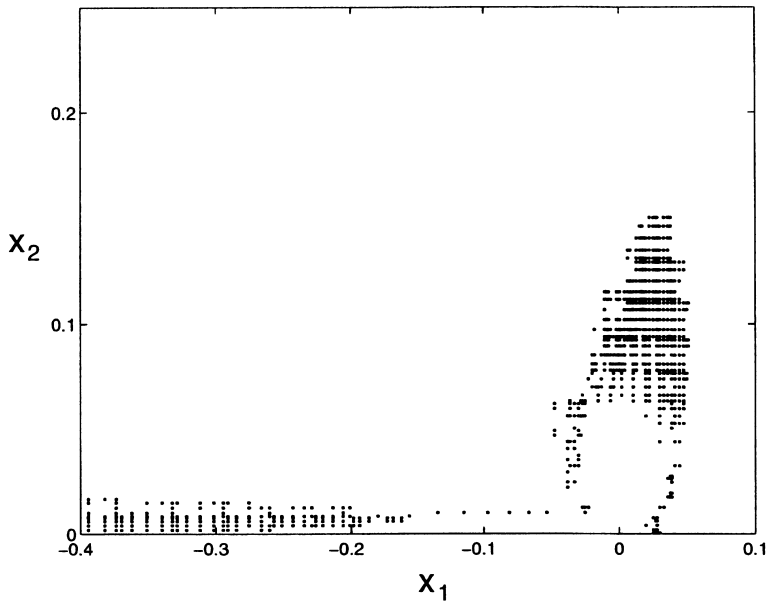

(a)

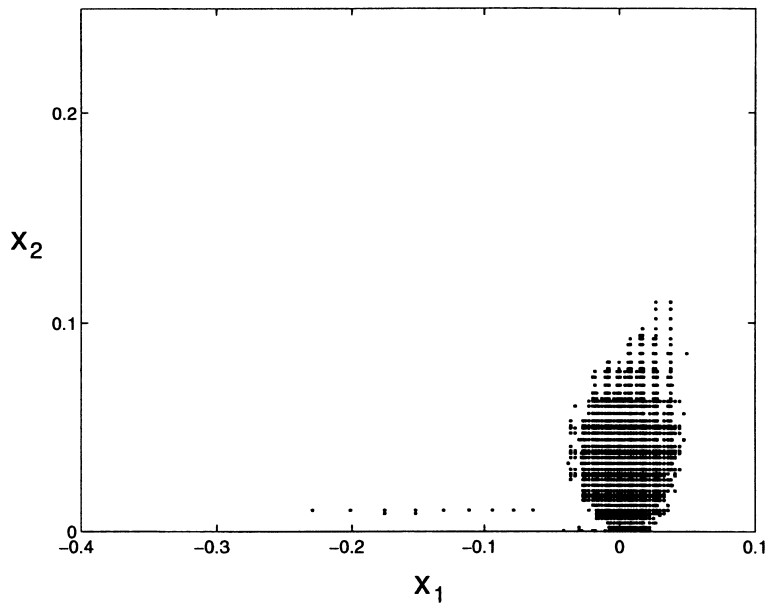

(b)

Fig. 18. The active plastic zones for $m_s = 0.3$, $Q = 50$ and $\xi = 0.1$: (a) low strain-rate zone; and (b) high strain-rate zone.

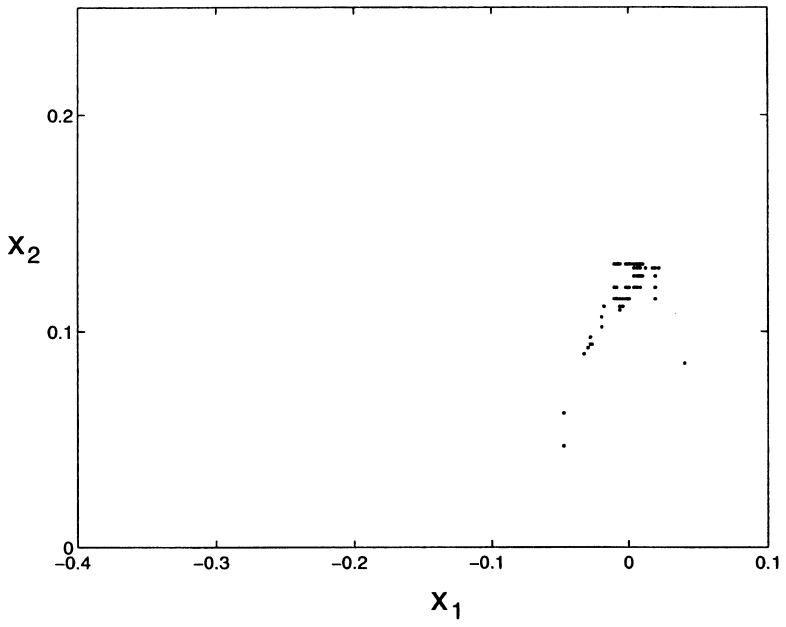

(a)

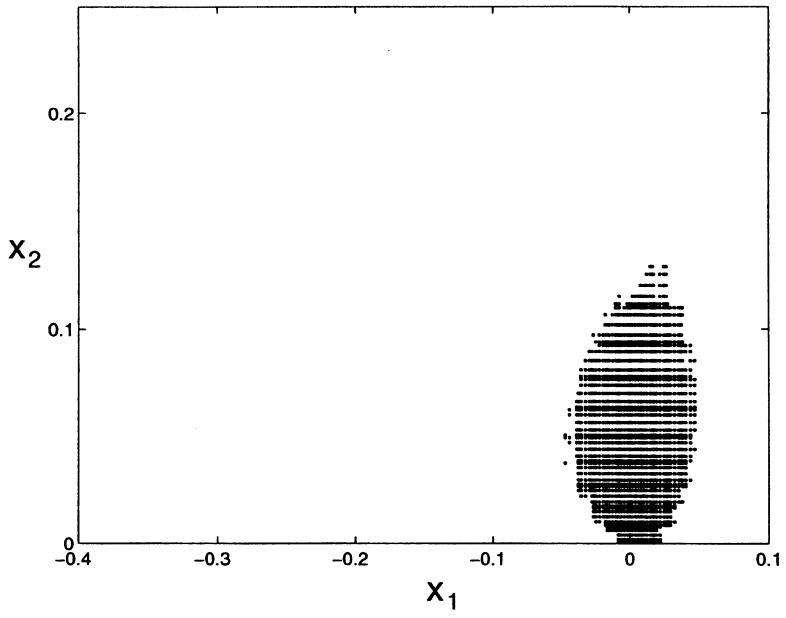

(b)

Fig. 19. The active plastic zones for $m_s = 0.3$, $Q = 10$ and $\xi = 0.1$: (a) low strain-rate zone; and (b) high strain-rate zone.

Table 2
G_{wake} for various combinations of m_s, ξ and Q

Q	50	35	20	5
$m_s = 0.2$ $\xi = 0.1$	0.0178	0.0164	0.0143	0.0037
$m_s = 0.4$ $\xi = 0.01$	0.0164	0.0127	0.0076	0.0011
$m_s = 0.4$ $\xi = 0.1$	0.0180	0.0144	0.0089	0.0015

may be considered as a measure of the overall driving force based on the material properties and characterizes the steady crack growth in viscoplastic materials. The points shown in Figs 18 and 19 correspond to the integration points that are at the yield state.

As shown in Fig. 18, for $Q = 50$, a reloading plastic zone occurs trailing the crack tip behind the active plastic zone. The results shown in Fig. 18 appear similar to those for rate-independent elastic–perfectly plastic materials. Since the response of the viscoplastic material model employed here reduces to that of the rate-independent elastic–perfectly plastic materials when Q approaches infinity (see Mataga et al., 1987), the similarity observed in Fig. 18 is reasonable. Unlike as in Fig. 18, there is no reloading plastic zone for $Q = 10$ as seen from the results in Fig. 19. With decreasing Q, the high strain-rate zone expands, and the low strain-rate zone shrinks simultaneously. The maximum vertical extent of the active plastic zone also decreases slightly. These observations indicate that the rate-dependent response of materials becomes dominant with decreasing Q.

(4) Examination of the assumptions in deriving asymptotic solutions

Two assumptions have been employed in the literature in deriving the analytical expression for G_{tip} presented by Freund and Hutchinson (1985) and Mataga et al. (1987). First, the residual elastic strain energy G_{wake} locked in the plastic wake is small enough to be neglected. Second, the plastic dissipation can be calculated using the near-tip stress distribution given in eqn (1) everywhere in the active plastic zone. The latter assumption implies that the plastic dissipation in the low strain-rate zone is small compared to that in the high strain-rate zone and it can be ignored. These assumptions are now examined using the numerical solutions obtained from the present formulation. The parameters, G_{wake}/G and r_{hs}, may be extracted from the numerical results where r_{hs} is the ratio of the energy dissipated in the high strain-rate zone to the total energy dissipated in the active plastic zone.

The parameter G_{wake}/G was computed using the line integral given in eqn (A.2) in the Appendix. The values of G_{wake}/G for various combinations of the material parameters ξ, Q and the crack speed m_s were given in Table 2. The contribution of G_{wake}/G is observed to be less than 1.8% for $Q \leqslant 50$ from this table. The variation of crack speeds m_s and of material parameters ξ only have a slight influence on G_{wake}/G. On the contrary, the material-loading parameter Q has a dominant effect on the variation of G_{wake}/G and it decreases remarkably with decreasing Q. That is, the residual elastic strain energy locked in the plastic wake decreases as the material response becomes more rate-dependent or more rate-sensitive. These observations indicate that it is reasonable to neglect the residual elastic strain energy locked in the plastic wake for high strain-rate crack growth (see Freund and Hutchinson, 1985).

The ratio r_{hs} may be computed using eqn (A.1) in the Appendix. The values of r_{hs} for various combinations of the material parameters ξ, Q and the crack speed m_s were given in Table 3. It is seen that the energy dissipated in the high strain-rate zone is usually more than 98% of the total energy dissipated in the active plastic zone. The ratio r_{hs} increases with increasing crack speeds m_s, decreasing material parameters ξ and decreasing material-loading parameters Q. In short, the ratio of the energy dissipated in the high strain-rate zone to the total energy dissipated in the active plastic zone increases as the rate response of the material becomes dominant in terms of increasing crack speeds, decreasing ξ and decreasing Q. Therefore, using the energy dissipated in the high strain-rate zone to represent the total energy dissipated in the active plastic zone is also a reasonable simplification for high strain-rate crack growth. It is noted, however, that these studies do not directly examine the second assumption.

(5) The relation between G_{tip} and G

As mentioned above, the main objective of numerical studies is to relate the crack-tip energy release-rate G_{tip} and the overall energy release-rate G, and to study the influence of the material parameters and the crack speeds on this relation. The non-dimensional crack-tip energy release-rate G_{tip}/G extracted from the numerical solutions is used to carry out these studies.

The variation of G_{tip}/G with Q corresponding to the material parameter $\xi = 0.1$ was obtained for crack speeds $m_s = 0.2$ and 0.4 and is shown in Figs 20(a) and (b), respectively. The two asymptotic solutions due to Freund and Hutchinson (1985) and Mataga et al. (1987) are also shown in these figures for comparison. As seen from these figures, for small Q, the difference between the two asymptotic solutions is small and the numerical results also provide a good agreement. As Q becomes large, the difference between the two asymptotic expressions increases and the numerical results deviate from these solutions. The numerical results, however, lie approximately in the middle of the two analytical results.

A comparison of the numerical predictions and the analytical results is shown in Fig. 21 where the crack-tip release-rate G_{tip}/G is plotted against the material-speed-loading parameter z defined in the Appendix. As seen in Fig. 21, the numerical results lie approximately in the middle of the two asymptotic ones. For G_{tip}/G below 0.5, there are lesser agreements as also observed by Mataga et al. (1987).

Table 3
The percentages occupied by the energy dissipated in the high strain-rate zone in the total energy dissipated in the active plastic zone

Q	50 (%)	35 (%)	20 (%)	5 (%)
$m_s = 0.4\ \xi = 0.01$	99.97	100	100	100
$m_s = 0.4\ \xi = 0.1$	96.58	98.16	99.45	99.96
$m_s = 0.2\ \xi = 0.1$	89.33	93.70	98.17	99.94

r_{hs}: The ratio of the energy dissipated in the high-strain-rate zone to the total energy dissipated in the active plastic zone.

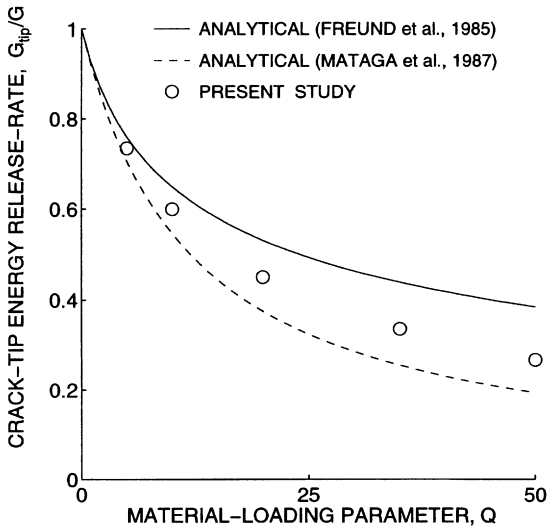

(a)

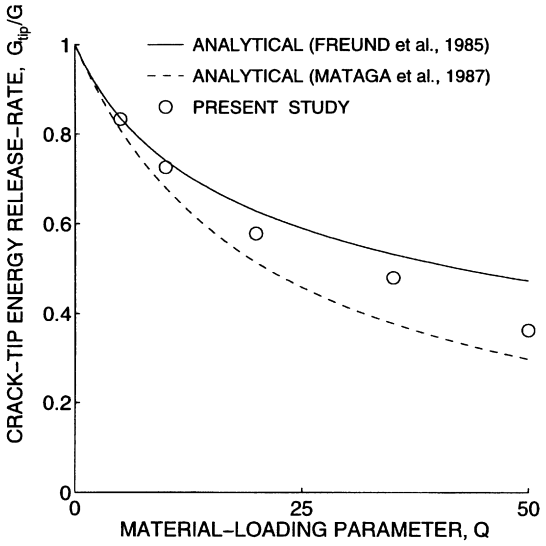

(b)

Fig. 20. The dependence of the crack-tip energy release rate G_{tip}/G on the crack-loading parameter Q for different crack speeds: (a) $m_s = 0.2$; and (b) $m_s = 0.4$.

7. Conclusion

An EFG based formulation for steady dynamic crack growth was developed in the present study. In this formulation, an extension of the convective mesh technique in FEM was employed

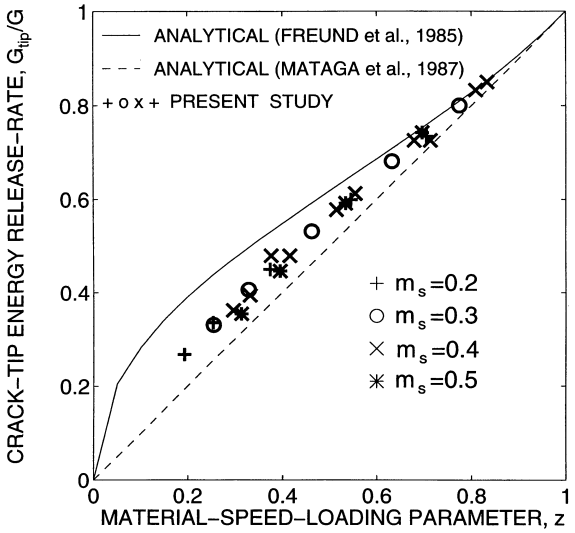

Fig. 21. Variation of the crack-tip energy release rate G_{tip}/G with the material-speed-loading parameter z.

to simulate the crack growth. Under the condition of small scale yielding, the elastic asymptotic stress or displacement field was imposed on the remote boundaries of the domain under consideration. The integration of constitutive equations was performed along the path line parallel to the direction of the crack growth made possible by the implicit requirement of the steady state condition. Based on the present formulation, a series of numerical solutions to steady dynamic growth problems of mode I cracks were obtained. The validity of the formulations was demonstrated by comparing the numerical solutions with available analytical solutions, and examining the theoretical invariants, such as the path-independent integral. Steady dynamic crack growth in rate-independent materials as well as rate-dependent materials was considered.

For steady dynamic crack growth in rate-independent materials, numerical results confirmed that crack speeds have an important influence. With increasing crack speeds, the existence of the elastic unloading wedge becomes apparent and the remote driving force required to propagate the crack increases. The numerical results for the first time revealed that the influence of strain hardening on steady dynamic crack growth in rate-independent materials shows the same trends as for steady quasi-static crack growth reported by Xu and Saigal (1997b).

For steady dynamic crack growth in rate-dependent materials, a comprehensive examination was made of the assumptions made in deriving the asymptotic solutions available in the literature (see e.g. Freund and Hutchinson, 1985; Mataga et al. 1987). Numerical results indicated that neglecting the residual elastic strain energy locked in the plastic wake and using the plastic dissipated energy in the high strain-rate zone instead of that in the entire active plastic zone are reasonable for high strain-rate crack growth. The material-loading parameter Q, which signifies the combined influence of the material properties and the overall driving forces, is a dominant parameter for determining the level of high strain-rate crack growth. The formula given by Freund and Hutchinson (1985) overestimates the crack-tip energy release rate G_{tip}/G, while the formula given by Mataga et al. (1987) underestimates it as the material-speed-loading parameter z decreases.

Acknowledgements

This work was supported under National Science Foundation Grant MSS-9057055. The encouragement from Professor Ted Belytschko of Northwestern University in utilizing the Element Free Galerkin methods is highly appreciated. Yu Xu is grateful to Dr Peter Mataga for many helpful discussions during this work and for all his assistance.

Appendix. Asymptotic analyses of high strain-rate crack growth

The near-tip behavior of high strain-rate cracks is characterized by eqns (1) and (2). The main objective in the analytical studies is to relate the crack-tip energy release-rate G_{tip} to the overall energy release-rate G. A general relation between G_{tip} and G was established by Freund and Hutchinson (1985) using a particular path-independent integral of the form

$$\frac{G_{\text{tip}}}{G} = 1 - \frac{1}{m_s}\int_A \sigma_{ij}\dot{\varepsilon}^p_{ij}\,\mathrm{d}A - \frac{G_{\text{wake}}}{G} \tag{A.1}$$

where A is the area of the active plastic zone; the second term on the right hand side represents plastic dissipation; and G_{wake} represents the residual elastic strain energy trapped in the plastic wake trailing the crack. The above equation represents a basic steady state energy balance relationship. The term G_{wake}/G can be expressed using a line integral as

$$\frac{G_{\text{wake}}}{G} = 2\int_0^h U_e^*\mathrm{d}x_2 = 2\int_0^h \lim_{x_1\to-\infty} U_e(x_1, x_2)\,\mathrm{d}x_2 \tag{A.2}$$

where $U_e(x_1, x_2)$ is the elastic strain energy density locked in the plastic wake; and h is the height of the plastic wake far behind the crack tip.

Two simplifications have been made in deriving the closed form expression for G_{tip}. One was to ignore the elastic strain energy locked in the plastic wake, i.e. to neglect the term G_{wake} in the above energy balance equation. The other was to use the near-tip stress distribution given by eqn (1) everywhere in the active plastic zone to calculate the plastic dissipation. This leads to the following closed form relationship between G_{tip} and G

$$\frac{G_{\text{tip}}}{G} = 1 - \frac{1}{3}D(m)(1+2\xi)\frac{\mu\dot{\bar{\gamma}}_0 G}{C_s\tau_y^2}\left(\frac{G_{\text{tip}}}{G}\right)^2 \tag{A.3}$$

with

$$D(m) = \frac{1}{2}\frac{H(m)}{m_s} \tag{A.4}$$

$$H(m) = \frac{2}{\pi^2}\frac{B(m)}{[(1-\nu)f(m)]^2} \tag{A.5}$$

$$B(m) = \int_{-\pi}^{\pi} [\tfrac{1}{2}\Sigma'_{ij}(\theta)\Sigma'_{ij}(\theta)]^2 \, \mathrm{d}\theta \tag{A.6}$$

$$\Sigma'_{ij} = \Sigma'_{ij} - \tfrac{1}{3}\Sigma_{ii} \tag{A.7}$$

Σ_{ij} and $f(m)$ may be found in the literature (see e.g. Freund, 1976; Freund and Hutchinson, 1985). Mataga et al. (1987) presented a modified formula for the relation for G_{tip} and G as

$$\frac{G_{\text{tip}}}{G} = \left[1 + \frac{1}{3} D(m)(1+2\xi)\frac{\mu\dot{\bar{\gamma}}_0 G}{c_2\tau_y^2}\right]^{-1} \tag{A.8}$$

The relation given in eqn (A.3) due to Freund and Hutchinson (1985) overestimates G_{tip}/G (underestimates the plastic dissipation), while relation in eqn (A.8) due to Mataga et al. (1987) underestimates G_{tip}/G (overestimates the plastic dissipation). Noting that both asymptotic relations depend on a single parameter $\frac{1}{3}D(m)(1+2\xi)(\mu\dot{\bar{\gamma}}_0 G/c_2\tau_y^2)$ and letting $z = [1+\frac{1}{3}D(m)(1+2\xi)(\mu\dot{\bar{\gamma}}_0 G/c_2\tau_y^2)]^{-1}$, which combines the influence of material parameters and crack speeds and will be termed in this study as the material-speed-loading parameter, the formula due to Mataga et al. (1987) can simply be expressed as

$$\frac{G_{\text{tip}}}{G} = z \tag{A.9}$$

The formula due to Freund and Hutchinson (1985) can be similarly rewritten as

$$\frac{G_{\text{tip}}}{G} = \frac{-z + \sqrt{4z - 3z^2}}{2(1-z)} \tag{A.10}$$

References

Achenbach, J. D., Kanninen, M. F. and Popelar, C. H. (1981a) Crack-tip fields for fast fracture of an elastic–plastic material. *Journal of the Mechanics and Physics of Solids* **29,** 211–225.

Achenbach, J. D. and Dunayevsky, V. (1981b). Fields near a rapidly propagating crack-tip in an elastic–perfectly plastic material. *Journal of the Mechanics and Physics of Solids* **29,** 283–303.

Akin, J. E. (1976) The generation of elements with singularities. *International Journal of Numerical Methods in Engineering* **10,** 1249–1259.

Belytschko, T., Lu, Y. Y. and Gu, L. (1994) Element-free Galerkin methods. *International Journal of Numerical Methods in Engineering* **37,** 229–256.

Brickstad, B. (1983) A viscoplastic analysis of rapid crack propagation experiments. *Journal of the Mechanics and Physics of Solids* **31,** 307–327.

Dean, R. H. and Hutchinson, J. W. (1980) Quasi-static steady crack growth in small-scale yielding. In *Fracture Mechanics*: 12*th Conference*, pp. 383–405. ASTM STP 700.

Drugan, W. J., Rice, J. R. and Sham, T. L. (1982) Asymptotic analysis of elastic–ideally plastic solids. *Journal of the Mechanics and Physics of Solids* **30,** 447–473.

Freund, F. B. (1976) The analysis of elastodynamic crack tip fields. In *Mechanics Today*, ed. S. Nemat-Nasser, **3,** 55–91. Pergamon Press, Oxford.

Freund, F. B. and Hutchinson, J. W. (1985) High strain rate crack growth in rate dependent solids. *Journal of the Mechanics and Physics of Solids* **33,** 169–191.

Freund, F. B., Hutchinson, J. W. and Lam, P. S. (1986) Analysis of high strain rate elastic–plastic crack growth. *Engng. Frac. Mech.* **23,** 119–129.

Gao, Y. C. and Nemat-Nasser, S. (1983). Dynamic fields near a crack tip growing in an elastic–perfectly plastic solid. *Mechanics of Materials* **2,** 47–60.

Lam, P. S. and Freund, L. B. (1983) Elastic–plastic finite element analysis of steady state dynamic crack growth in plane strain tension. Brown University, MRL E-149.

Lam, P. S. and Freund, L. B. (1985) Analysis of dynamic growth of a tensile crack in an elastic–plastic material. *Journal of the Mechanics and Physics of Solids* **33,** 153–167.

Leighton, J. T., Champion, C. R. and Freund, L. B. (1987) Asymptotic analysis of steady dynamic crack growth in an elastic–plastic material. *Journal of the Mechanics and Physics of Solids* **35,** 541–563.

Lo, K. K. (1983) Dynamic crack tip fields in rate sensitive solids. *Journal of the Mechanics and Physics of Solids* **31,** 287–305.

Mataga, P. A. (1986) High strain-rate crack growth. Ph.D. thesis, Harvard University.

Mataga, P. A., Freund, L. B. and Hutchinson, J. W. (1987) Crack tip plasticity in dynamic fracture. *J. Phys. Chem. Solids.* **48,** 985–1005.

Ostlund, S. (1990) On numerical modeling and fracture criteria of dynamic elastic–viscoplastic crack growth. *International Journal of Fracture* **44,** 283–299.

Parks, D. M., Lam, P. S. and McMeeking, R. M. (1981) Some effects of inelastic constitutive model on crack tip fields in steady quasi-static growth. In *Advances in Fracture Research*, ed. D. Francois, **5,** 2607–2614. Pergamon Press.

Shenoy, V. B. and Krishna, K. R. (1994) Dynamic crack growth in a power hardening viscoplastic material. *Journal of Engineering Materials and Technology* **116,** 465–470.

Slepyan, L. I. (1976) Crack dynamics in an elastic–plastic body. *Mekhanika Tverdogo Tela* **11**.

Xu, Y. (1996) The element free Galerkin formulation for steady crack growth. Ph.D. thesis, Carnegie Mellon University.

Xu, Y. and Saigal, S. (1997a) An element free Galerkin formulation for stable crack growth in an elastic solid. *Computer Methods in Applied Mechanics and Engineering*, to be published.

Xu, Y. and Saigal, S. (1997b) An element free Galerkin study of steady quasi-static crack growth in plane strain tension in elastic–plastic materials. *Computational Mechanics*, to be published.